ACS OMEGA

Open Access

http://pubs.acs.org/journal/acsodf

Article

Quantification of Enzymatic Biofilm Removal Using the Sauerbrey Equation: Application to the Case of *Pseudomonas protegens*

Ivana K. Levy,* Débora Salustro, Fernando Battaglini, Leonardo Lizarraga, Daniel H. Murgida, Rosalía Agusti, Norma D'Accorso, Dorotea Raventos Segura, Lorena González Palmén, and R. Martín Negri

Cite This: *ACS Omega* 2024, 9, 10445−10458

Read Online

ACCESS | Metrics & More | Article Recommendations | Supporting Information

ABSTRACT: A methodology for the quantitative analysis of enzymatic removal of biofilms (BF) was developed, based on a quartz crystal microbalance (QCM) under stationary conditions. This was applied to the case of *Pseudomonas protegens* (PP) BFs, through a series of five enzymes, whose removal activity was screened using the presented methodology. The procedure is based on the following: when BFs can be modeled as rigid materials, QCM can be used as a balance under stationary conditions for determining the BFs mass reduction by enzymatic removal. For considering a BF as a rigid model, energy dissipation effects, associated with viscoelastic properties of the BF, must be negligible. Hence, a QCM system with detection of dissipation (referred to as QCM with dissipation) was used for evaluating the energy losses, which, in fact, resulted in negligible energy losses in the case of dehydrated PP BFs, validating the application of the Sauerbrey equation for the change of mass calculations. The stationary methodology reduces operating times and simplifies data analysis in comparison to dynamic approaches based on flow setups, which requires the incorporation of dissipation effects due to the liquid media. By carrying out QCM, glycosidase-type enzymes showed BF removal higher than 80% at enzyme concentration 50 ppm, reaching removal over 90% in the cases of amylase and cellulase/xylanase enzymes. The highest removal percentage produced a reduction from about 15 to 1 μg in the BF mass. Amylase enzyme was tested from below 50 to 1 ppm, reaching around 60% of removal at 1 ppm. The obtained results were supported by other instrumental techniques such as Raman spectroscopy, attenuated total reflection Fourier transform infrared spectroscopy, atomic force microscopy, high performance anion exchange chromatography, thermogravimetric analysis, and differential scanning calorimetry. The removal quantifications obtained with QCM were compared with those obtained by well-established screening techniques (UV−vis spectrophotometry using crystal violet and agar diffusion test). The proposed methodology expands the possibility of using a quartz microbalance to perform enzymatic activity screening.

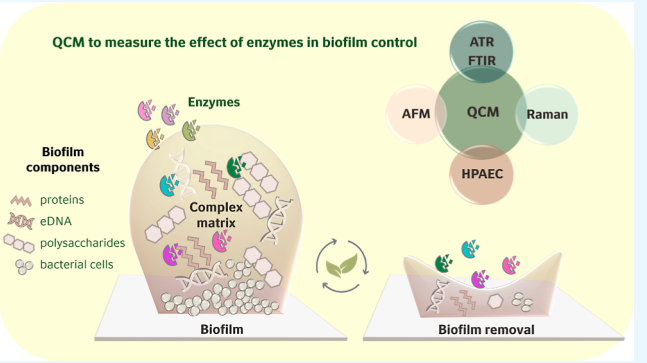

1. INTRODUCTION

The microorganisms in biofilms (BFs) live in a self-produced matrix of hydrated extracellular polymeric substances (EPS). EPS are mainly constituted by polysaccharides, proteins, nucleic acids, and lipids, forming a three-dimensional interconnected network that mediates adhesion to a substrate.[1] Bacterial BFs, compared to their planktonic counterparts, show an increased resistance to environmental stress and antimicrobials because of multiple causes and mechanisms.[2] This has driven an urgent search for new innovative strategies for both BF removal and prevention. One of the most sustainable approaches is the application of aqueous-soluble macromolecules with a range of functionalities that can impact BF integrity, including enzymes, peptides, proteins, synthetic polymers, and nanomaterials.[3−6] Due to the high complexity and diversity of BFs, identifying green solutions for each case is a challenge.

Another key aspect in BF research is the development of methodologies for the detection and removal evaluation BF. The development of new methodologies adaptable for quantifying BF removal and BF mass on different surfaces has great relevance since it is known that BF characteristics are influenced by the type of substrate,[7] its chemical nature,[8−10]

Received: October 26, 2023
Revised: November 30, 2023
Accepted: January 3, 2024
Published: February 20, 2024

topographic pattern,[11] roughness,[12,13] and hydrophobicity,[14,15] among others characteristics.

The 96-well microtiter plate assay used for UV−vis analysis of BFs with crystal violet (CV) is one of the most widely used methods for assessing BF formation because of its robustness and high screening capacity.[16,17] However, the CV method presents some drawbacks for applications, for example, in those cases where there is a weak BF adhesion to the plate, or when there are colorimetric interferences affecting the measurements.[18]

Alternatively, although less explored for BF research, quartz crystal microbalance (QCM) is an extremely sensitive technique, suitable for multiple types of surfaces. The key component is quartz, a piezoelectric material. To fabricate quartz crystal resonators, wafers are cut from the bulk quartz crystal at specific orientations, with respect to the crystallographic axis. The quartz discs used in QCMs are mostly processed using the "AT cut" that provides pure thickness shear mode oscillation where the two surfaces of the crystal move in an antiparallel fashion. After the disc was cut, a pair of metal electrodes is directly evaporated on the top and bottom surfaces of the quartz disc. When the corresponding alternating current is applied to the quartz disc, it oscillates at its resonance frequency is in the order of MHz.[19]

The frequency of oscillation is affected by the addition or removal of small amounts of mass onto the electrode surface. Thus, QCM can be applied for measuring surface mass density (mass per unit area), in nanogram to microgram level in mass on a surface.[20] When a rigid film is deposited, the mass variation on the electrode surface is linearly related to the change of the oscillation frequency (frequency shift) through the well-known Sauerbrey Equation. In these cases, there is a full coupling of the deposited mass to the crystal oscillation,[21,22] which is typical for molecular adsorption via the vacuum or gas phase. However, in a liquid environment, molecular adsorption on the crystal can include contributions from the media by hydration/solvation and/or entrapment of molecules within the adsorbed film, producing soft or viscoelastic films. The resulting layer may not fully couple to the oscillating crystal, leading to dampening or energy loss of the oscillation. Hence, the mass of such films cannot be determined accurately by measuring only the frequency change. Both frequency change (ΔF) and energy loss (measured as the dissipation change, ΔD) need to be measured to accurately determine the mass change of a viscoelastic film. This technique is called QCM with dissipation (QCM-D),[23,24] and it has received increasing interest, especially in biosensors research, with promising development of mass-sensitive viral and small biomolecules diagnostic devices. QCM is a mass-sensitive device which offers label-free detection of analytes. Thus, a QCM transducer coated with a specific receptor is able to detect frequency shifts associated with receptor−analyte interaction and analyte recognition.[25] In many cases, molecularly imprinted polymers, artificial materials that generate surface modifications, have been used as an alternative to antibody's or antigen's recognition layer.[26,27]

Kartal et al.[28] described the preparation of an insulin-imprinted poly(hydroxyethyl methacrylate)-*N*-methacryloyl-(L)-histidine methyl ester-based QCM sensor for insulin determination in real time. The whole protocol cycle for performing one measurement and determining the analyte mass takes a relatively long time, about 50 min, due to the processes of adsorption, desorption, and regeneration of the modified surface sensor.

Chernyshev and Skliar[29] introduced an interesting application of QCM in real time as a biosensor on air, quantifying the amount of extracellular vesicles in a drop of volatile solvent. Mujahid et al.[30] comprehensively reviewed acoustic transducers, including QCM, surface acoustic wave, and film bulk acoustic resonators, comparing their sensitivity and reliability with more classical analytical instruments According to the authors, the main advantages of acoustic devices as QCM are the ability to monitor extremely low mass shifts, label-free detection of specific analytes, and small instrumental size.[30] Particularly, in BF research, QCM-D has been extensively applied for dynamic studies in liquid medium, under flow conditions in real time.[31,32] Thus, QCM-D experiments have been mainly applied for analysis of BF development deposit and attachment of bacteria,[15,33] BF removal mechanisms,[34] and the effect of environmental conditions on BFs[35,36] in a liquid environment in real time. These studies require a high control of experimental conditions and complex physicochemical models for data interpretation.

Recently, Kaga et al.[37] studied the removal of a β-glucan film by surfactants, showing that QCM-D allows to assess the BF removal in real time, by monitoring the viscoelasticity of the β-glucan films. However, since experiments were performed under flow in a liquid environment, the data treatment becomes more complex.

Therefore, the main objective of the present work is to develop a simple methodology, including sample preparation, measurements conditions, and data analysis, for quantitative evaluation of early stage BF removal by enzymes, based on QCM measurements under stationary conditions.[38,39] This objective was aimed to contribute to protocols that do not require dynamic measurements under flow conditions. The stationary methodology on air reduces operating times and simplifies data analysis in comparison to dynamic approaches based on flow setups, which require incorporating dissipation effects since working with liquid media. The presented protocol constitutes a novelty, as far as we know.

For this purpose, it is demonstrated that dehydrated *Pseudomonas protegens* (PP) BFs behave as rigid films, where energy dissipation is negligible, thus validating the conditions for using the Sauerbrey equation to determine the percentage of enzymatic removal. This allows applying a simplified measuring protocol and data treatment, in comparison with applications of QCM-D in flow cell viscoelastic models for BF removal studies.[34,40] *P. protegens*, a microorganism of relevance in microbial induce corrosion processes, was selected for testing the developed approach.[41,42] A selection of enzymes, targeting the different components of the BF matrix and/or bacteria cells, was evaluated for removal. For supporting the most remarkable results obtained by QCM, methodologies for well-established techniques were optimized: the conventional spectrophotometric method with CV, vibrational spectroscopies as Raman spectroscopy (RS) and attenuated total reflectance for Fourier transform infrared spectroscopy (ATR-FTIR),[43,44] atomic force microscopy (AFM),[45−48] high performance anion exchange chromatography (HPAEC),[49,50] thermogravimetric analysis (TGA), differential scanning calorimetry (DSC),[51] and agar diffusion test.[52]

To the best of our knowledge, this is the first publication presenting a simple methodology for quantitative BF removal

https://doi.org/10.1021/acsomega.3c08475
ACS Omega 2024, 9, 10445−10458

studies based on QCM measurements under stationary conditions.

2. MATERIALS AND METHODS

2.1. Chemicals. All the enzymes were supplied by Novozymes A/S, Denmark: an amylase, two serine endoproteases (SE I and SE II), a cellulase/xylanase, and a peroxidase. Stock solutions were made in PBS 1× (buffer phosphate solution, pH 7.3−7.5) from Biopack reagents.

For LB medium preparation, yeast extract and tryptone were obtained from Britania Laboratories, and sodium chloride was obtained from Biopack. For M63 minimal medium with 0.4% arginine, H_2PO_4, K_2HPO_4, and $MgSO_4$ were provided by Biopack, $(NH_4)_2SO_4$ was supplied by Anedra, and L-arginine free base was provided by Sigma-Aldrich. Deionized water was obtained by a Double Pass Reverse Osmosis System (Wasserteck, Argentina), with a resistivity of 1.5 MΩ cm. CV and sugar standards for HPAEC were provided by Sigma-Aldrich.

2.2. Cultures. Gram-negative bacteria *P. protegens Pf-5*[53] was used (referred as PP along the text) in all the experiments. From a fresh agar plate, PP colonies were inoculated in sterile aqueous LB medium, and this suspension was incubated overnight at 250 rpm at room temperature (RT). Then, the overnight PP liquid culture was diluted to an optical density of 0.1 (at 600 nm) in LB medium. This suspension with OD 0.1 was used as the inoculum and again incubated during 24 h at RT in LB together with the surface used as the substrate in each technique.

Bacterial viability, estimated by the conventional method of serial dilutions and plate count, determined that OD 0.1 corresponds to CFU 10^7−10^8.

2.3. QCM Studies. *2.3.1. Instrumental Conditions.* A Q-Sense E1 system from Biolin Scientific was used to perform the QCM-D measurements. Gold-coated 4.95 MHz AT-cut quartz crystals (QSX 301, Q-Sense, Göteborg, Sweden) were used as substrates for BF growth. Crystals have 0.3 mm of thickness, 14 mm diameter, and roughness less than 3 nm. Before measurements, crystals were placed in the sample holder of the equipment and left to stabilize at 25.00 (±0.05) °C.

2.3.2. BF Growth on the Surface of the QCM Crystal. Crystals for QCM were pretreated according to routine cleaning protocols and irradiated with UV/O_3 for 15 min before use.[32] Clean crystals were identified and measured by QCM at least two times to obtain the baseline values for each crystal before the incubation experiments. After this, clean QCM crystals were incubated at RT in a 24-well plate (Jet Biofil), and 1 mL of inoculum OD 0.1 in LB medium was added. In the case of the enzymatic treatments, the enzyme was added at t = 24 h at the desired concentration and left in incubation to act for 1 h. After incubation, each identified crystal was removed from the well, rinsed four times with sterilized deionized water to wash away medium and planktonic bacteria, and dried with $N_2(g)$, and measured again. The same protocol was performed in all crystals to assume similar losses by dehydration.

2.3.3. Measurements and Data Processing. QCM crystals can be excited to resonate at several different harmonics, labeled with a number 'n'. The available harmonics are the fundamental, n = 1, and a set of overtones to the fundamental, n > 1. The fundamental is the harmonic with the lowest resonance frequency that it is possible to excite, and the overtones resonate with a frequency that is higher than the fundamental. For AT-cut QCM crystals, which oscillate in the thickness shear mode, only the odd harmonics (n = 1, 3, 5, etc.) are possible to excite electrically. For example, for this case, the fundamental mode is 5 MHz, then the overtones resonate at odd multiples of the fundamental, i.e., 15, 25, 35 MHz, etc.[54] In addition, the dissipation energy (D_n) of the crystal is determined, and it is related to the inverse of the time involved in the decay of each frequency amplitude when the excitation is stopped. Rigid films present a small ΔD_n, close to zero, and no spreading of the values for the different overtones. On the contrary, in the case of flowing films, ΔD_n increases, having different values for the different overtones.

When a BF is deposited on the surface of the crystal, a shift in the resonance frequency (and its overtones) and dissipation factors are observed. The response of a QCM device as shift in frequency (ΔF) is given for eq 1

$$\Delta F = \frac{-f_0^{\,2}\,\Delta m}{A\sqrt{\rho\mu}} \tag{1}$$

where f_0 is the fundamental resonant frequency of QCM, Δm is the mass change per unit of crystal area, A is the piezoelectrically active area of QCM in cm^2, ρ is the density of quartz (2.648 g/cm^3), and μ is the shear modulus of an AT-cut quartz crystal (2.947×10^{11} $g/cm\ s^2$).

Although the present work was performed completely on air, it is worth mentioning that for measurements in a liquid environment, the acoustic properties of the liquid must be considered, giving the following equation (eq 2)

$$\Delta F = -f_0^{\,3/2}\sqrt{\frac{\rho_l \eta_l}{\pi\rho\mu}} \tag{2}$$

where ρ_l and η_l are the density and the viscosity of the liquid, respectively.[25]

In the protocol presented here, only measurements under air (no liquid environment) and static conditions are considered. Therefore, the following analysis is based on eq 1. As is known, each overtone has a frequency shift defined as ΔF_n. The so-called normalized shift, ΔF, given by $\Delta F_n/n$, is expected to have a constant value, independent of the overtone. The presence of the deposited mass introduces also shifts of the dissipation factors, referred to as dissipation shifts, ΔD_n. If the dissipation shifts remain relatively low, then the deposited surface mass density of BF (mass by unit of the crystal area), referred to as Δm, is proportional to ΔF according to the Sauerbrey equation, which is a reorganization of eq 1, adapted for mass density determinations, giving the eq 3.[22]

$$\Delta m = -C\frac{\Delta F_n}{n} = -C\Delta F \tag{3}$$

where n is the considered overtone number and C is a constant that depends on the property of the crystal. For the used 4.95 MHz AT-cut quartz crystal at room temperature, the C is approximately equal to 17.7 $ng/(cm^2{\cdot}Hz)$.

Therefore, the Sauerbrey equation relates the surface mass density of the BF to the frequency shifts. The calculated surface mass density of the BF must be independent of the overtone used for its calculation. In practice, five overtones were considered, and the arithmetic average of the surface mass density was calculated. Only in few cases, the overtone number 1 was ruled out and four overtones were considered for being numerically more consistent. The instrument provides the frequencies as a function of time (sensorgrams);

https://doi.org/10.1021/acsomega.3c08475
ACS Omega 2024, 9, 10445−10458

hence, the mass deposited on the crystal can be determined from the frequency difference between the baseline of the clean crystal (before incubation) and the frequency of the crystal after incubation.[55] Resonant frequency and dissipation were registered for 1−3 min to observe QCM data quality, regarding to noise and drifts, and recorded by Qsoft software. The values of the resonance frequency were used to calculate the mass grown. As expected, the resonance frequency decreases after incubation with respect to the clean crystal, according to the added mass. Figure 1 shows normalized frequency (F/n) vs time for the fifth overtone before incubation (clean crystal) and after incubation (the crystal after BF growth and subsequent enzymatic treatment). Line in dots schematizes how the frequency is affected according to the degree of removal: frequency becomes more similar to a clean crystal when the removal is higher (less mass is attached) and frequency is going down, increasing the delta, when removal is lower (more mass is attached).

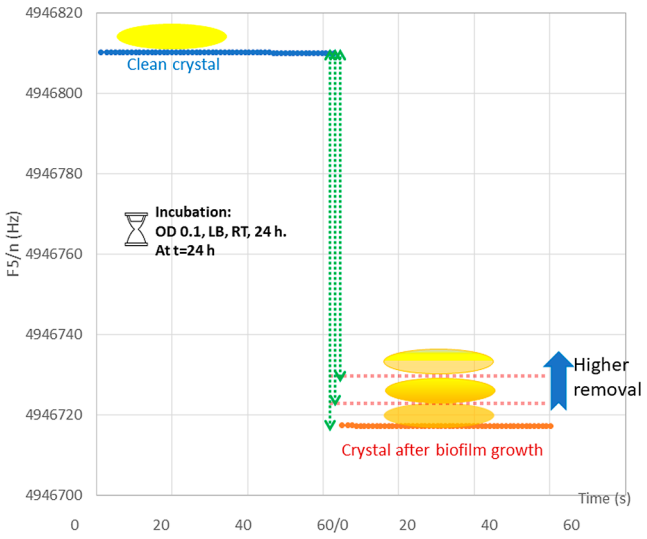

Figure 1. Normalized frequency (F/n) vs time for the fifth overtone showing the delta between the frequency before incubation (clean crystal) and after incubation (crystal after BF growth and subsequent enzymatic treatment).

For this purpose, first, values for F and D for n = 1, 3, 5, 7, and 9 were recorded for the clean sensor. These measurements were performed in at least by duplicate. Each frequency was normalized by dividing by n.

Then, the sensor was incubated in the 24-well plate with PP and, after the described procedure above, the frequency shift values were recorded again. These measurements were performed at least in duplicate also. Finally, the subtraction of frequencies between the clean sensor and the sensor after incubation allowed to obtain, by the Sauerbrey equation, a surface mass density for each overtone, and the result was averaged. The validity of the criterion was verified for the subtraction and for the values before the subtraction. The rationale for choosing multiple overtones is to acquire surface mass density values for each overtone to be averaged. Furthermore, this approach enables the monitoring of the system's behavior as a rigid film.

The percentage difference of surface mass density before and after incubation is calculated according to eq 4

$$\%\ \text{removal (QCM)} = \left[1 - \frac{m_{\text{untreated BF}} - m_{\text{enzyme treated BF}}}{m_{\text{untreated BF}}}\right] \times 100\% \quad (4)$$

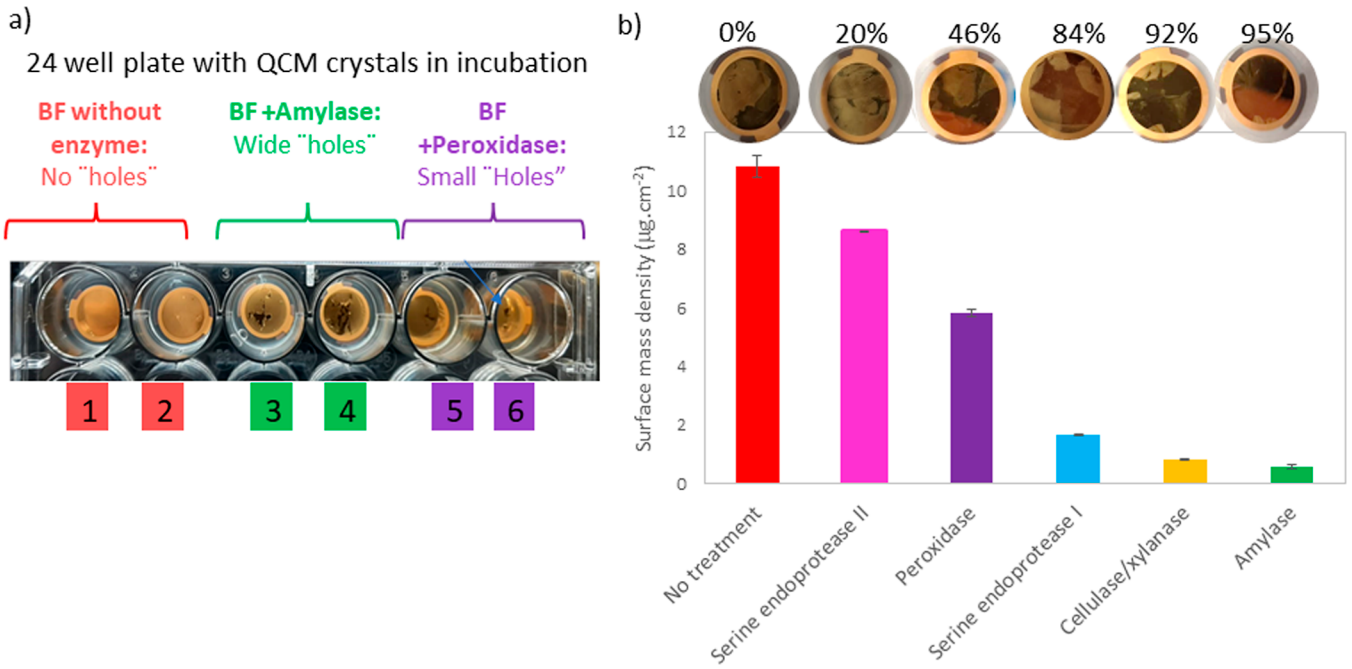

Figure 2. (a) Top view of the wells some minutes after enzyme addition. (b) BF surface mass density obtained from QCM measurements 1 h after of the enzyme addition (50 ppm in all cases) and a photograph of each crystal after treated, rinsed, and dried. Conditions: LB medium, 24 h of incubation, and RT. The altitude of each bar is an average over several replicates ($N \geq 3$), where the value for an individual sample is obtained as average over the different overtone. The errors associated with the bars were calculated as the standard deviation of the values when considering the replicates.

https://doi.org/10.1021/acsomega.3c08475
ACS Omega 2024, 9, 10445−10458

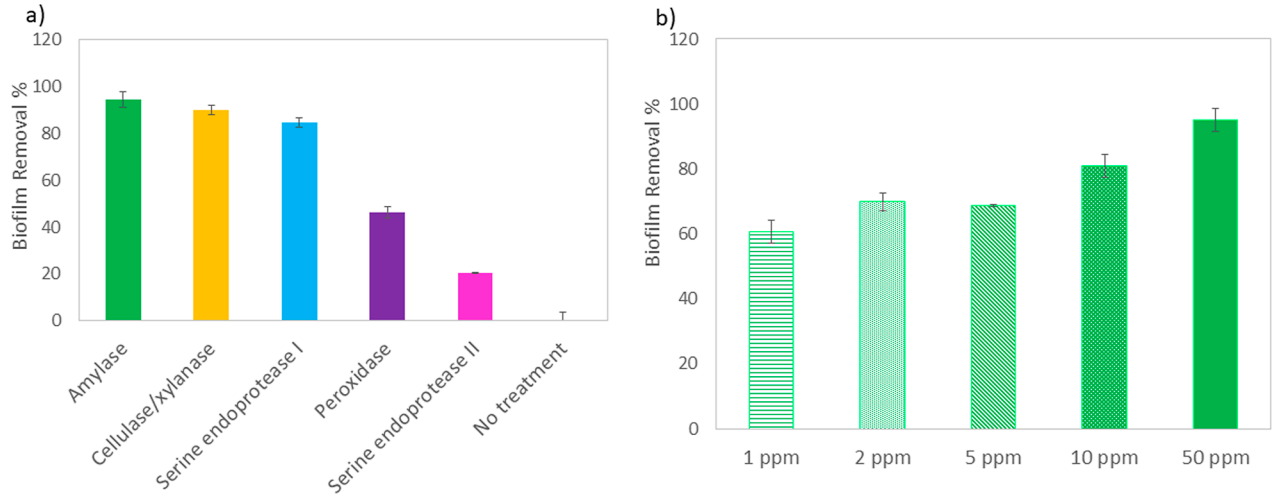

Figure 3. Removal percentage determined by QCM after 1 h using (a) enzymes at 50 ppm. (b) Using amylase enzyme at doses from 1 to 50 ppm. Conditions: LB medium, 24 h of incubation, RT. Errors for % removal were calculated as % coefficient of variation (% coefficient of variation = 100 × standard deviation/media).

It is important to note that in eq 4, the area of the crystal and C constant are canceled and the removal has the same expression using deposited mass or surface mass density. The values of area (A) and C are only taken into account for absolute mass calculations, i.e., the mass deposited before and after the treatment with enzyme.

Crystals incubated with LB medium (blank) did not show shifts in comparison with clean crystals, indicating that LB adsorption is not detectable. Samples for QCM were prepared at least in triplicate, QCM measurements were performed at least in triplicate, and the results were averaged. Each BF removal experiment was repeated at least 3 times.

To be more concise, materials and methods for the techniques used to support QCM results are presented in the Supporting Information.

3. RESULTS AND DISCUSSION

3.1. Enzymatic Removal Determined by QCM. The QCM crystals incubated with enzymes showed visible BF removal after the first few minutes of the enzyme addition (Figure 2a). In wells 1 and 2, the BFs without treatment look like an opaque layer over the crystal. The wells 5 to 6, treated with peroxidase, showed "holes" on the BF layer. The holes were wider on the BF treated with amylase (wells 3 and 4).

Once the crystals were rinsed with water and dried with N_2, the aspect of the BF is shown in Figure 2b. In the same figure, the surface mass density and the % of removal calculated are illustrated.

In Figure 2b, surface mass density is reported. The altitude of each bar is an average over several replicates ($N \geq 3$), where the value for an individual sample is obtained as average over the different overtones. The errors associated with the bars were calculated as the standard deviation of the values when considering the replicates. The decrease in mass due to the enzymatic activity was remarkable. BF mass decreases by a factor of 10, from about 15 to 1 μg, approximately (area of the crystal = 1.53 cm^2).

Figure 3 shows the results as % removal with the error estimation. All the enzymes tested showed the ability to remove BF at a concentration of 50 ppm (Figure 3a). Amylase, cellulase/xylanase, and serine endoprotease I were the most efficient with values of 95, 92, and 90% removal, respectively. To further study the correlation between removal and enzyme concentration, we chose the most active enzyme, amylase, to perform this determination (Figure 3b). Although the removal percentage decreased when decreasing the enzyme concentration, removal remained above 60% even at a low concentration of enzyme such as 1 ppm. Between 1 and 5 ppm, the concentration variation is very small and the % removals are in a range of 55 to 70% considering the error. It is worth noting that amylase and cellulase/xylanase are glycosidases that act on polysaccharides and glycoproteins, modifying their structures and physical properties.

Errors for % removal were calculated as % coefficient of variation (% coefficient of variation = 100 × standard deviation/media).

3.2. Suitability for QCM Analysis. As was mentioned, when using the Sauerbrey equation, the film must be *rigid*. This hypothesis is considered valid when: (i) $\Delta F_n/n$ is independent of the overtone order and (ii) ΔD_n is very small relative to $\Delta F_n/n$.[56] Numerically, it is assumed when the ratio between dissipation shift and the frequency shift is less than 4×10^{-7}.[23] The validity of this assumption was verified for all the considered overtones by calculating the ratio between dissipation shift and the frequency shift for each determination and for the subtraction where ΔD= (D after incubation- D before incubation) and $\Delta F/n$ = (F/n after incubation − F/n before incubation). Figure 4 illustrates the fulfillment for a set of data even taking into account stricter criteria of less than 5×10^{-8} Hz^{-1}, proposed in refs 57 and 58.

Another key aspect for the reliability of the determinations is that the difference of the normalized frequencies ($\Delta F_n/n$) must be greater than the signal drifts. Figure 5 and Table 1 illustrate this aspect.

The repeatability between two measurements on the same day for a given sample is illustrated in Figure 6.

It is important to remark that temperature stabilization in the sample holder (at 25.00 ± 0.05 °C) before measurements minimized the drift effects considerably.

The technique presents an excellent sensitivity. For instance, frequency shifts around 10^{-3}% ($\Delta F/F$) were easily detected.

https://doi.org/10.1021/acsomega.3c08475
ACS Omega 2024, 9, 10445−10458

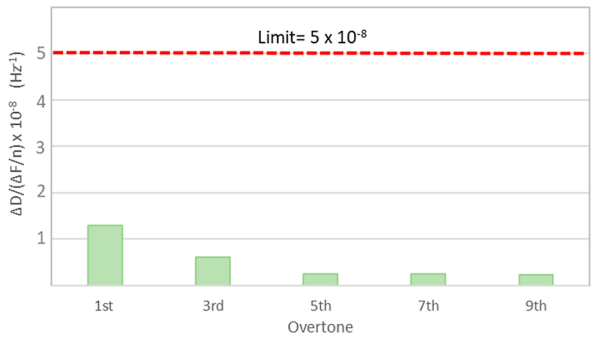

Figure 4. Calculations for quantitative criterion with limit 5×10^{-8} Hz^{-1} for using the Sauerbrey equation, where ΔD = (D after incubation − D before incubation) and $\Delta F/n$ = (F/n after incubation − F/n before incubation). Conditions: BF treated with amylase 1 ppm. Instrumental error is around 0.1 Hz for a frequency determination and around 0.2 Hz for the difference delta.

As was mentioned, each BF removal experiment was repeated at least three times with at least three replicates for sample. The standard deviation in the surface mass density calculated considering all the data set for a sample was typically less than 0.15, and the coefficient of variation considering the surface mass density average of all the data set for a given sample was in all cases less than 4%.

3.3. Enzymatic Removal Determined by UV−vis Spectrophotometry and Agar Diffusion Test. BF removal (%) was obtained for each treatment by subtraction of the corresponding blank to the absorbance at 600 nm (A), according to eq 5

$$\%\ \text{BF removal} = \left[1 - \frac{A_{\text{treated sample}} - A_{\text{treated sample blank}}}{A_{\text{positive control}} - A_{\text{positive control blank}}}\right] \times 100\% \quad (5)$$

The selected culture media for these experiments was M63 minimal media. Details concerning the comparison between M63 minimal media and LB media are provided in Supporting Information (Figure S1).

Removal results obtained by UV−vis (Figure 7) showed that amylase was the most efficient enzyme, followed by cellulase/xylanase, consistent with QCM results. However, unlike QCM, the UV−vis technique did not allow for a good differentiation of activity between the other enzymes.

All the removal experiments with UV−vis spectrophotometry were repeated at least three times. Results were averaged, and standard deviations were calculated. Error in % removal was estimated as % variation coefficient (% standard deviation/average). The standard deviation between experiments of removal considering replicates analyzed on different days was around 10%.

Additionally, agar diffusion tests were performed (Figure S2). The halo was considered as the zone where some grade of inhibition around the disk with enzyme was noticed under magnifying glass. The halos were modeled by an ellipse, and the observed dimensions are listed in Table S1.

Figure 8 shows a representation of the removal observed by taking the ratio between the ellipse area for each treatment and the ellipse area for the PBS blank (solvent of the enzyme). The size of each sphere is related to the observed ratio. Results show the highest removal for amylase and the lowest for serine endoprotease II (SEII), consistently with the results obtained by QCM. Intermediate cases follow the ranking of removal observed by QCM, although with lower differentiation between enzymes.

3.4. Supplementary Studies of Removal with Amylase by Additional Techniques. *3.4.1. Carbohydrate Analysis and Sugar Content of the EPS by HPAEC.* The carbohydrate analysis of the extracted EPS in the BFs, before and after treatment, showed a substantial reduction of the total carbohydrate content from 0.22 mg mL^{-1} in the untreated sample to 0.12 mg mL^{-1} after treatment with amylase (Conditions: 50 ppm amylase for 1 h, LB medium, incubation time 24 h, RT).

Figure 9a shows the chromatograms obtained by HPAEC for both samples after acid hydrolysis (see sample preparation in the Supporting Information). Sugar composition, calculated by integration of the areas in the chromatogram, is expressed as relative percentages in Figure 9b,c.

Glucose was the most abundant sugar component in the BF, followed by glucosamine and fucose. Other sugars detected were xylose, arabinose/galactosamine, galactose, and rhamnose.

As is known, amylase hydrolyzes α-(1−4)-linked glucose residues present in polysaccharides. As a result, glucose

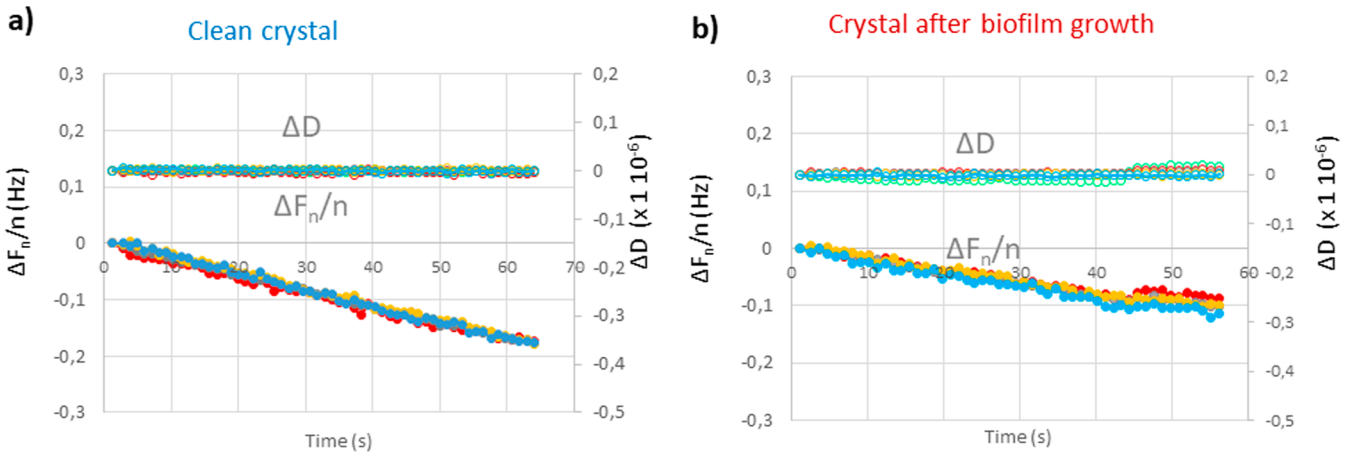

Figure 5. Drift observed (signal vs time) for overtones third to ninth for (a) clean crystal and (b) crystal after BF growth with enzyme added at a low concentration ([amylase] = 1 ppm).

https://doi.org/10.1021/acsomega.3c08475
ACS Omega 2024, 9, 10445−10458

Table 1. Values for F_n (Not Normalized) and D at the End of the Measurements before and after Incubation and the Shifts in the Resonance Frequency[a]

	before incubation		after incubation		shifts		
n	F_n (Hz)	$D_n \times 10^{-6}$	F_n (Hz)	$D_n \times 10^{-6}$	ΔF_n (Hz)/n	$\Delta D_n \times 10^{-6}$	$\Delta D_n \times 10^{-6}/(\Delta F_n/n)$
3	14843227.9	15.455	14842989.2	15.9425	−796	0.4875	-6.13×10^{-10}
5	24734002.4	11.505	24733603.7	11.7075	−797	0.2025	-2.54×10^{-10}
7	34623421.7	8.39	34622855.4	8.59	−809	0.2	-2.47×10^{-10}
9	44513793.9	6.71	44513060.1	6.895	−815	0.185	-2.27×10^{-10}

[a]BFs treated with [amylase] = 1 ppm.

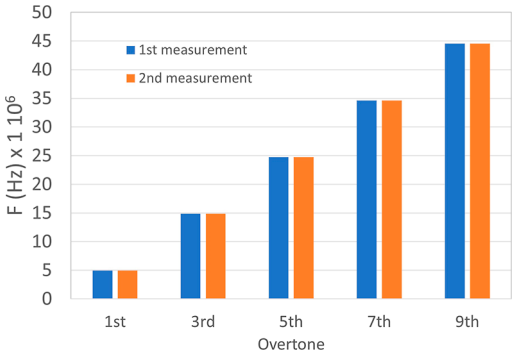

Figure 6. Outcome of two measurements of frequency performed for the same clean QCM crystal at the start of the measurements and after all measurements of the day. Instrumental error is around 0.1 Hz for frequency determinations.

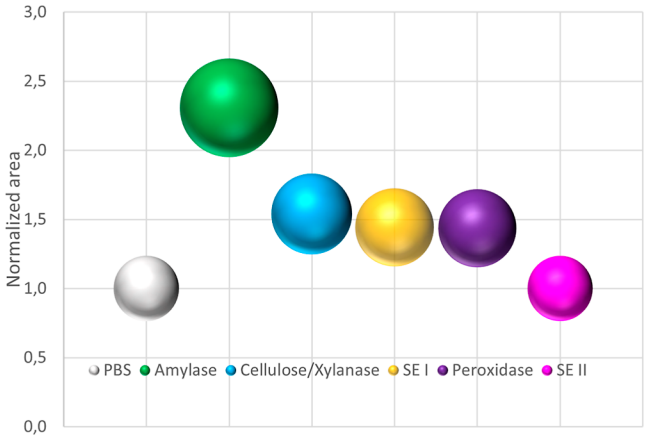

Figure 8. Normalized halo area for each treatment (ratio between the ellipse area for each treatment and the ellipse area for the PBS blank). The size of each sphere is related to the ratio observed.

monomers are produced and washed out in the dialysis step of the isolation protocol. Thus, after the enzymatic treatment, glucose decreases in its relative percentage while glucosamine, an unknown compound, and some other monosaccharides increase their relative percentages. Apparently, the degradation of glucose is not complete. This agrees with the presence of other residues different from glucose since amylase is an exoglycosidase that could cleave the polysaccharide up to the point of ramification with other monosaccharides. Glucosamine, on the other hand, could come from partial deacetylation of *N*-acetylglucosamine in the acid hydrolysis.

It is worth noting that monomers are detected because the polysaccharides are isolated and then hydrolyzed to analyze monosaccharide composition. Enzymatic hydrolysis is prior to isolation, so those released by amylase are lost in dialysis (see Experimental details in Materials and Methods in Supporting Information).

3.4.2. Raman Spectroscopy. The use of RS for BF detection is based on the presence of largely dominant broad bands from ca. 1200 to 2000 cm^{-1}. This spectral region

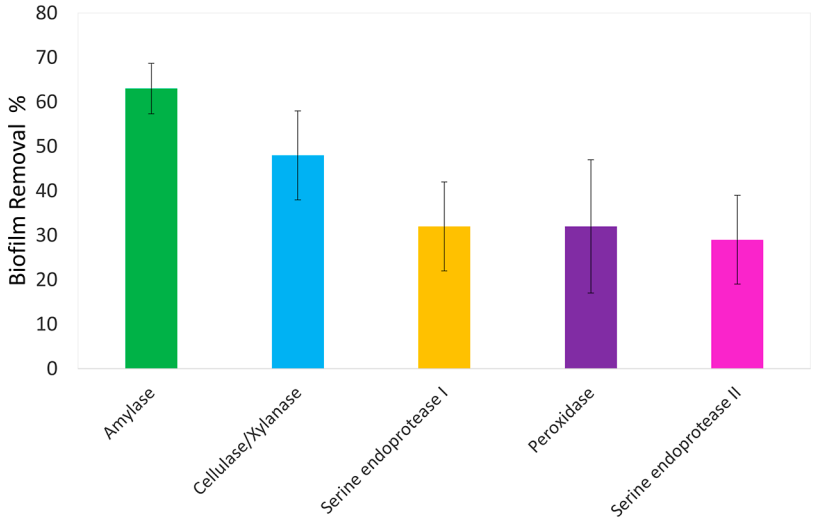

Figure 7. Removal percentage by UV−vis spectrophotometry with CV for the tested enzymes at 1000 ppm, after 1 h of treatment. Conditions: M63 minimal media, incubation time 24 h, RT. Errors for % removal were calculated as % coefficient of variation (% coefficient of variation = 100 × standard deviation/media).

https://doi.org/10.1021/acsomega.3c08475
ACS Omega 2024, 9, 10445−10458

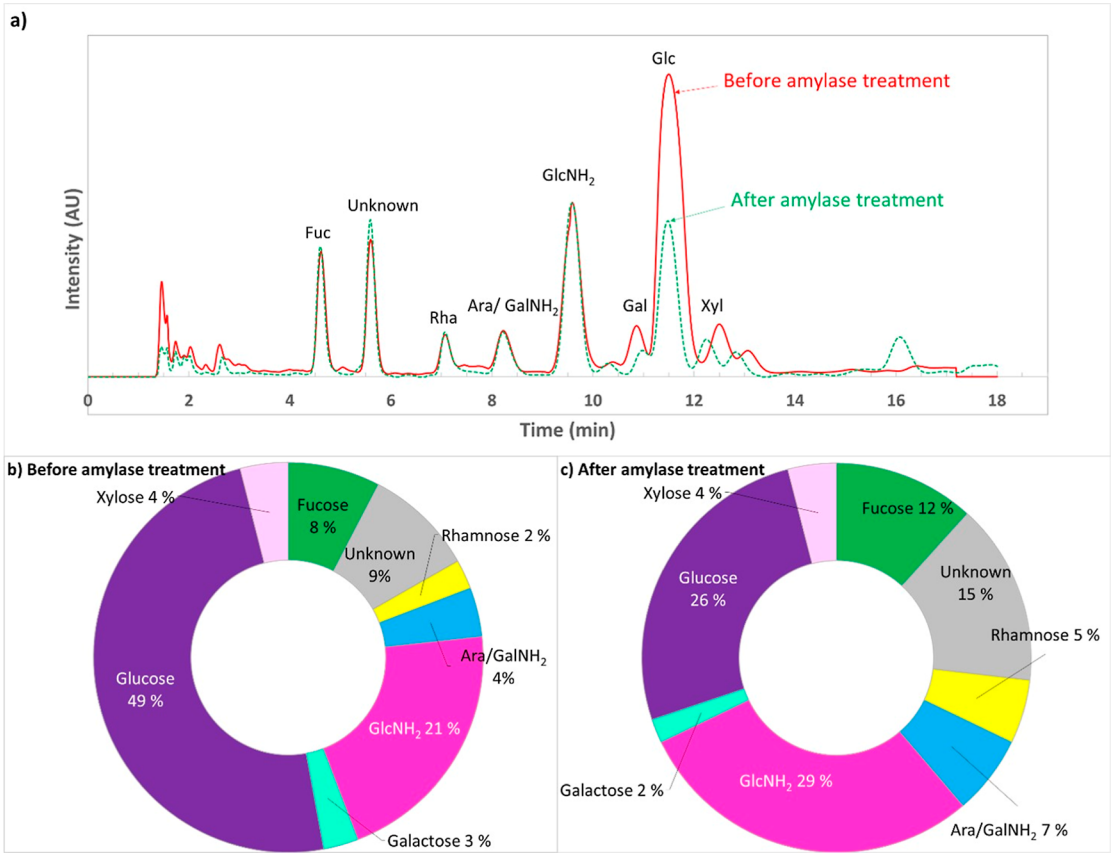

Figure 9. (a) Chromatograms for a sample of BF not treated and treated with amylase. Relative area (%) for (b) sample of BF not treated and (c) sample of BF treated with amylase.

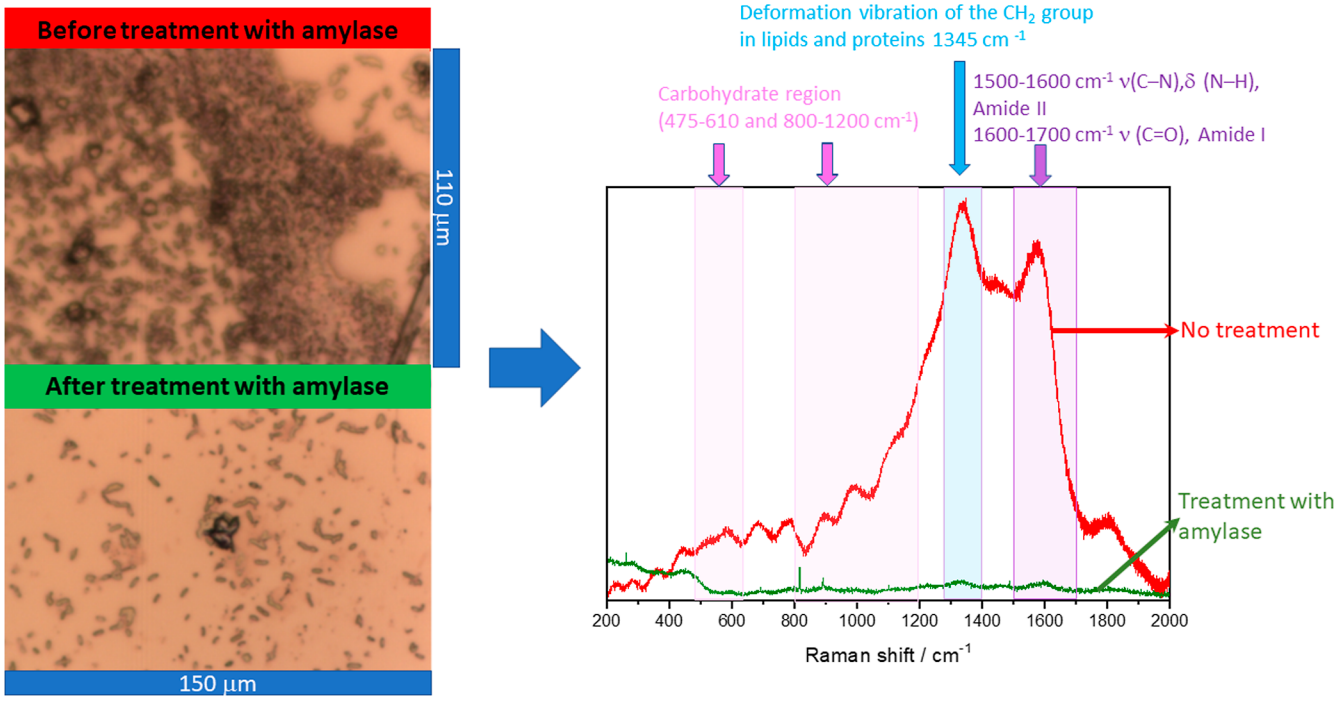

Figure 10. Optical images and Raman spectra for a BF without treatment and a BF treated with amylase. Raman conditions: wavelength 532 nm, 20 obj., 50% laser intensity (100% = 5 mW).

comprises overlapping bands from different cellular and extracellular components, such as ν(C═O) amide I and ν(C−N)/δ(N−H) amide II bands from proteins in the 1500−1700 cm^{-1} range and CH_2 deformations at ca. 1345 cm^{-1} and ν(C═C) in the 1600−1500 cm^{-1} region from lipids and proteins.[43,44] Raman bands from carbohydrates are expected in

https://doi.org/10.1021/acsomega.3c08475
ACS Omega 2024, 9, 10445−10458

the 475−610 and 800−1200 cm^{-1} regions.[59] DNA bands, mainly originating from the ring breathing modes of cytosine, thymine, uracil, as well as ν_s (O−P−O) bands from the phosphodiester bonds are expected in the low frequency region, mostly at around 780 cm^{-1}.[60] Usually, the complex pattern of multiple overlapping bands does not allow for a reliable assignment of each signal to a specific normal mode; however, the overall spectral intensity scales with the density of the BFs. Optical images and Raman spectra were obtained for BFs before and after treatment with amylase (Figure 10). The signals appear within the range expected for the different chemical components of the BFs, and the dense colonies that comprised the BF provide high intensity signals before amylase. On the other hand, the sample treated with amylase shows few and small growing areas with depleted colonies and low intensity of signals.

An equivalent analysis for a sample treated with peroxidase is shown in Figure S3 in the Supporting Information. The optical image shows a depletion of the BF for the treated sample and a decrease of the band intensities in the spectra, although less pronounced than those described for amylase. These findings are consistent with those of QCM, indicating the superior effect of amylase over the peroxidase for BF removal.

It is worth mentioning that the use of QCM crystals as substrates for Raman is a good strategy for providing spectra without background or substrate signals, allowing for the detection of the BF and the removal effect.

3.4.3. ATR-FTIR. ATR-FTIR analysis for a BF and BFs treated with amylase or peroxidase is shown in Figure 11. Band

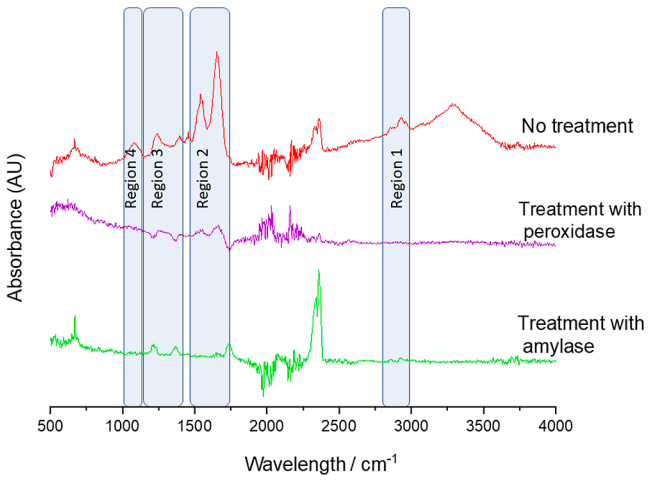

Figure 11. ATR-FTIR spectra and regions for the characteristic functional groups for a BF without treatment, a BF treated with amylase, and a BF treated with peroxidase.

assignments are given in Table 2. There are four defined regions in the BF ATR-FTIR spectra, assignable to (1) fatty acids, (2) peptide and protein structures, (3) phospholipids and of nucleic acids, and (4) polysaccharides.[61] The signals between 2200 and 2400 cm^{-1} are known as signals of carbon dioxide in air. The intensity of the bands is considerably decreased due to the enzymatic treatment in the four characteristic regions of the BF spectra. In particular, the Amide II band at 1550 cm^{-1} can be used for estimation of total biomass of the proteins, because it is free of interferences from water. This band decreases significantly with the treatments,

Table 2. ATR-FTIR Band Assignment[61]

region	wavenumber [cm^{-1}]	band assignment
	3400	OH of water
1. fatty acid region	2956	CH_3 asym. stretch
	2920	CH_2 asym. stretch
	2870	CH_3 sym. stretch
	2850	CH_2 sym. stretch
2. protein region	1745/1735	>C═O stretch, ester, fatty acids
	1705	>C═O stretch, ester, carboxylic groups
	1652−1648	amide I, (C═O) different conformation
	1550−1548	amide II, N−H, C−N and structure of proteins
	1460−1454	C−H bend. from CH_2
3. mixed region	1400−1398	C−O bend. from carboxylate ions
	1303	amide II (C−N)
	1240	P═O from phosphate
	1222	P═O
	1114	C−O−P, P−O−P
4. polysacch. region	1085	ring vibrations
	1052	C−O, C−O−C from polysaccharides

having a lower intensity for the case of the treatment with amylase than for the peroxidase.

The outcomes by ATR-FTIR are in line with those obtained by the other techniques, and the analysis of these bands could be used to provide a qualitative indication of enzymatic removal degree.

3.4.4. AFM Analysis. Bacterial coverage differences between surfaces can be appreciated by using atomic force microscopy. In our case, the comparison between surfaces without treatment (control) or treated with amylase or peroxidase showed that surface covered decreased visibly after enzymatic treatments, being amylase more effective than peroxidase (Figure 12).

The images were used to calculate the degree of surface coverage by measuring the area covered by bacteria and referring it to the total area of each image using the Gwyddion software (see more details in Supporting Information). Samples treated with amylase showed 8% of coverage in comparison with 28% for peroxidase and 55% for non-treated samples, resulting in removal percentages of 85% for amylase and 50% for peroxidase. These results are in good accordance with those of QCM (95% for amylase and 46% for peroxidase). However, it is important to take into account that using AFM, only a small percentage of the total area is analyzed, while QCM detects the total amount of material on the whole surface.

3.4.5. Thermal Analysis. 3.4.5.1. Thermal Gravimetric Analysis. Analysis by thermal gravimetry under a nitrogen atmosphere of a BF without enzymatic treatment showed multiple degradation steps, one below 100 °C and other two from above 100 °C up to 600 °C (Figure S4). The first step corresponds to the loss of retained water because of the hydrophilic character of the BF. The second step is due to the initial decomposition and loss of small molecules, and the third step corresponds to the degradation of polysaccharides.[62] Finally, the plateau corresponds to the inorganic materials present in the sample. The thermogram indicates the complex structure of the BF. The sample treated with amylase, on the

https://doi.org/10.1021/acsomega.3c08475
ACS Omega 2024, 9, 10445−10458

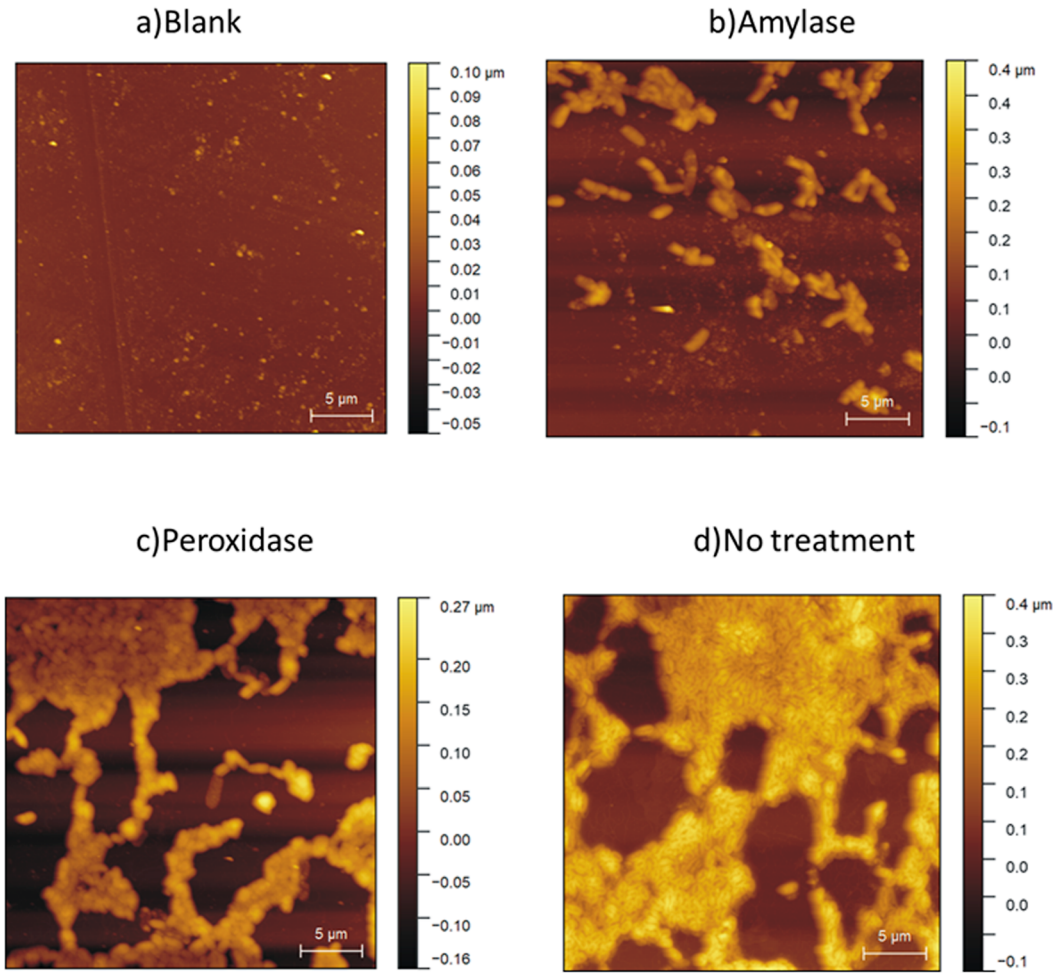

Figure 12. AFM images for (a) LB medium (blank), (b) BF treated with amylase, (c) BF treated with peroxidase, and (d) BF without treatment. AFM height images are expressed in vertical axes.

other hand, decomposed in a single stage as a consequence of degradation of the polysaccharides (Figure S4).

3.4.5.2. Differential Scanning Calorimetry. DSC studies showed a significant decrease of the glass transition temperature (T_g) from 120 to 80 °C for a BF without enzymatic treatment vs a BF treated with amylase (Figure S5a,b, respectively). It is known that smaller molecules have minor T_g than bigger ones, and this is in accordance with the initial complex structure of the BF being dramatically degraded by the glucose enzymatic removal with amylase.

Therefore, both thermal analysis techniques, TGA and DSC, contribute to the BF characterization, showing evidence of BF removal.

4. CONCLUSIONS

The implemented methodology, based on the Sauerbrey equation in a stationary configuration, was able to provide quantitative determinations of enzymatic removal with an excellent discrimination of enzymatic activity among the considered enzymes. The PP BFs were modeled by a rigid-material model, since energy dissipation effects were negligible. The QCM methodology was used to obtain the absolute masses of the developed BFs. Moreover, the results showed that the analysis of only one overtone shift could provide accurate information for enzymatic screening, decreasing instrumentation cost and data processing time. The results of the enzymatic screening performed with our approach point out glycosidases as the more efficient among the considered enzymes. The quantitative analysis using the Sauerbrey equation indicates that high removal percentages can be obtained with glycosidases at relatively low concentrations.

Polysaccharides constitute the major components of the EPS matrix; hence, it is worth clarifying its degradation mechanism. As it was previously reported for Gram-negative bacteria, polysaccharide intercellular adhesion is attributed to poly *N*-acetyl glucosamine (PNAG), the β-(1,6)-linked PNAG being the major component of the exopolysaccharides of BFs produced by *Pseudomonas fluorescens* and *Escherichia coli*, among others.[63,64] Similarly, *Pseudomonas aeruginosa* BFs contain three different polysaccharides, namely, Pel, Psl, and alginate (Figure S6). Recent studies have proposed that Pel is a cationic exopolysaccharide with 1,4-linked partially de-*N*-acetylated *N*-acetylgalactosamine.[65] Psl is a polymer consisting in repeating units of a pentasaccharide containing D-mannose, D-glucose, and L-rhamnose.[66] In this context, enzymes capable of degrading the polysaccharides by the cleavage of the glycosidic bonds are expected to weaken *Pseudomonas* BFs significantly.

Amylase and cellulase and xylanase are glycoside hydrolases (GHs). In the case of amylase, it catalyzes the cleavage of the α-(1,4) glycosidic bonds of glucose in starch, glycogen, and several other oligosaccharides. Cellulase catalyzes hydrolysis of

https://doi.org/10.1021/acsomega.3c08475
ACS Omega 2024, 9, 10445−10458

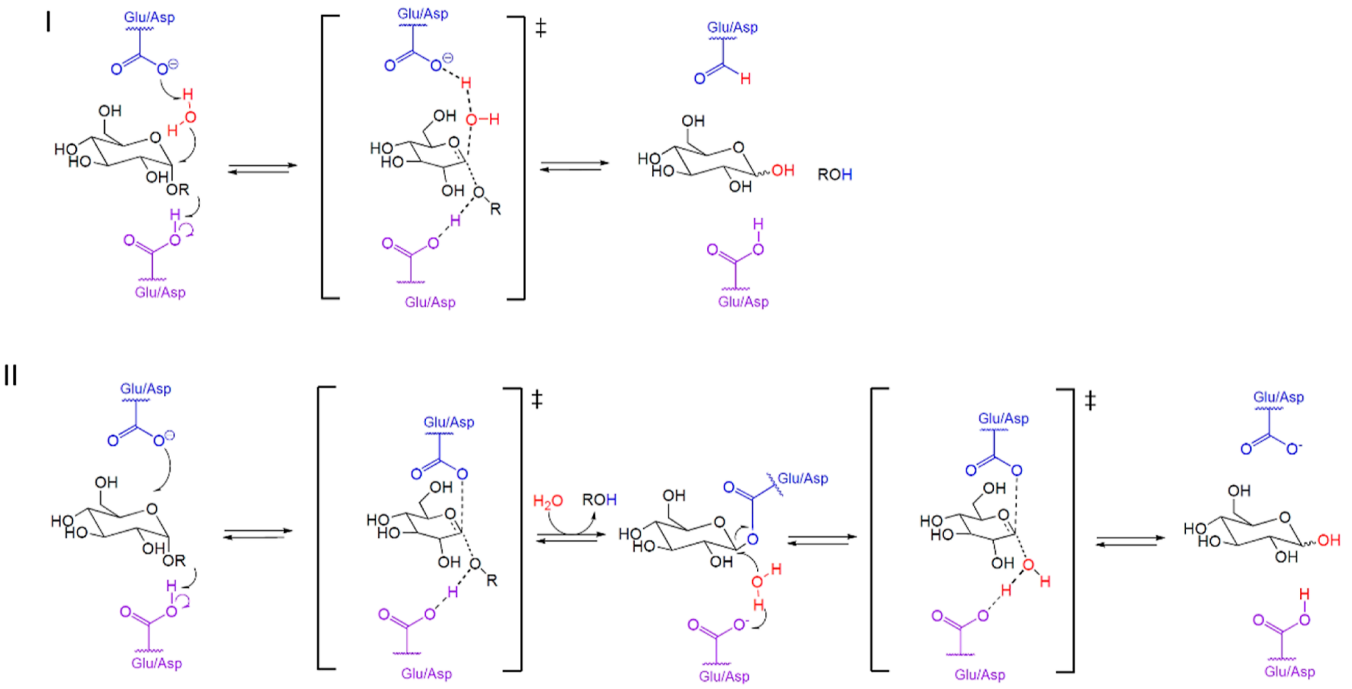

Figure 13. Mechanisms of cleavage of glycosidic linkages of polysaccharides in BFs by GH enzymes: (I) mechanism of GH by a concerted pathway and (II) mechanism of GH by formation of an enzyme−substrate covalent intermediate.

the β-(1,4) glycosidic bonds of glucose, which is one of the most found linkages in the exopolysaccharides of BF formed by various species, such as *P. aeruginosa*, *E. coli*, *S. aureus*, *Salmonella enterica*, among others.[67]

GHs enzymes follow the general acid−base catalysis involving conserved Asp/Glu residues to cleave the glycosidic linkages of the polysaccharides of the BF.[67] A scheme of two plausible mechanisms is shown in Figure 13.

The analysis by HPAEC and the results of removal obtained with the implemented techniques are consistent with the postulated mechanisms. Thereby, the presented analysis and mechanisms indicate that GH enzymes, such as amylase and cellulase/xylanase, can be a solution for the effective removal of many BFs by attacking the main components of the EPS in the BF.

The methodology presented in this article can be applied to different QCM crystals commercially available (quartz crystal coated with different metals and compounds) and also customizable crystals by surface modifications. This opens a wide perspective for studies of BF removal on a variety of surfaces used in many industries and medicine.

■ ASSOCIATED CONTENT

Data Availability Statement

All data generated or analyzed during this study are available from the corresponding author on reasonable request.

Supporting Information

The Supporting Information is available free of charge at https://pubs.acs.org/doi/10.1021/acsomega.3c08475.

The file includes additional experimental details, materials and methods, complementary results obtained by the techniques UV−vis, Raman and ATR-FTIR, agar diffusion test, TGA and DSC, HPAEC, and AFM (PDF)

■ AUTHOR INFORMATION

Corresponding Author

Ivana K. Levy − *Instituto de Química Física de los Materiales, Medio Ambiente y Energía (INQUIMAE). Consejo Nacional de Investigaciones Científicas y Técnicas (CONICET), Universidad de Buenos Aires (UBA), Buenos Aires C1428EGA, Argentina;* orcid.org/0000-0003-0260-1857; Email: ilevy@qi.fcen.uba.ar, ivanaklevy@gmail.com

Authors

Débora Salustro − *Instituto de Química Física de los Materiales, Medio Ambiente y Energía (INQUIMAE). Consejo Nacional de Investigaciones Científicas y Técnicas (CONICET), Universidad de Buenos Aires (UBA), Buenos Aires C1428EGA, Argentina*

Fernando Battaglini − *Instituto de Química Física de los Materiales, Medio Ambiente y Energía (INQUIMAE). Consejo Nacional de Investigaciones Científicas y Técnicas (CONICET), Universidad de Buenos Aires (UBA), Buenos Aires C1428EGA, Argentina; Universidad de Buenos Aires (UBA), Departamento de Química Inorgánica, Analítica y Química Física. Facultad de Ciencias Exactas y Naturales, Buenos Aires C1428EGA, Argentina;* orcid.org/0000-0002-1113-1642

Leonardo Lizarraga − *Universidad de Buenos Aires (UBA), Departamento de Química Inorgánica, Analítica y Química Física. Facultad de Ciencias Exactas y Naturales, Buenos Aires C1428EGA, Argentina; Centro de Investigación en Bionanociencias (CIBION), Consejo Nacional de Investigaciones Científicas y Técnicas (CONICET), Buenos Aires C1425FQD, Argentina*

Daniel H. Murgida − *Instituto de Química Física de los Materiales, Medio Ambiente y Energía (INQUIMAE). Consejo Nacional de Investigaciones Científicas y Técnicas (CONICET), Universidad de Buenos Aires (UBA), Buenos Aires C1428EGA, Argentina; Universidad de Buenos Aires*

https://doi.org/10.1021/acsomega.3c08475
ACS Omega 2024, 9, 10445−10458

(UBA), Departamento de Química Inorgánica, Analítica y Química Física. Facultad de Ciencias Exactas y Naturales, Buenos Aires C1428EGA, Argentina; orcid.org/0000-0001-5173-0183

Rosalía Agusti − *Centro de Investigaciones en Hidratos de Carbono (CIHIDECAR), Consejo Nacional de Investigaciones Científicas y Técnicas (CONICET), Universidad de Buenos Aires, Buenos Aires C1428EGA, Argentina; Universidad de Buenos Aires (UBA), Departamento de Química Orgánica, Facultad de Ciencias Exactas y Naturales, Buenos Aires C1428EGA, Argentina;* orcid.org/0000-0003-2825-9009

Norma D'Accorso − *Centro de Investigaciones en Hidratos de Carbono (CIHIDECAR), Consejo Nacional de Investigaciones Científicas y Técnicas (CONICET), Universidad de Buenos Aires, Buenos Aires C1428EGA, Argentina; Universidad de Buenos Aires (UBA), Departamento de Química Orgánica, Facultad de Ciencias Exactas y Naturales, Buenos Aires C1428EGA, Argentina*

Dorotea Raventos Segura − *Novozymes A/S, Lyngby 2800, Denmark*

Lorena González Palmén − *Novozymes A/S, Lyngby 2800, Denmark*

R. Martín Negri − *Instituto de Química Física de los Materiales, Medio Ambiente y Energía (INQUIMAE). Consejo Nacional de Investigaciones Científicas y Técnicas (CONICET), Universidad de Buenos Aires (UBA), Buenos Aires C1428EGA, Argentina; Universidad de Buenos Aires (UBA), Departamento de Química Inorgánica, Analítica y Química Física. Facultad de Ciencias Exactas y Naturales, Buenos Aires C1428EGA, Argentina;* orcid.org/0000-0003-1427-7927

Complete contact information is available at: https://pubs.acs.org/10.1021/acsomega.3c08475

Author Contributions

I.K.L.: Conceptualization, data curation, methodology, validation, formal analysis, investigation, writing—original draft, writing—review and editing, visualization, supervision, project administration, measurements, processing and data treatment, and general discussion. D.S.: BF samples preparation and UV−vis measurements. F.B.: QCM interpretation and discussion. L.L.: AFM measurements, resources, and general discussion. D.H.M.: Raman measurements and discussion. R.A.: HPAEC measurements and discussion. N.D.: Conceptualization, writing—review and editing and general discussion. D.R.S.: UV−vis method discussion. L.G.P.: Conceptualization, resources, writing—review and editing, project administration, funding acquisition, and general discussion. R.M.N.: Conceptualization, resources, writing—review and editing, project administration, funding acquisition, and general discussion. All authors have read and approved the final manuscript.

Notes

The authors declare no competing financial interest.

■ ACKNOWLEDGMENTS

I.K.L., L.L., F.B., D.H.M., R.A., N.D., and R.M.N. are research members of the National Council of Research and Technology (CONICET, Argentina). Financial support was received from Novozymes A/S (Denmark), University of Buenos Aires (UBACyT projects 20020150100079BA, 20020190100297BA, 20020190100226BA, and 20020190200245BA), CONICET (PIP 2021-2023 11220200100993CO, and 11220200100410CO), and Ministry of Science, Technology, and Innovations (MINCYT-FONCYT, Argentina, PICT-2020-SERIEA-00710).

■ REFERENCES

(1) Flemming, H. C.; Wingender, J. The BF matrix. *Nat. Rev. Microbiol.* **2010**, *8* (9), 623−633.

(2) Li, Y.; Xiao, P.; Wang, Y.; Hao, Y. Mechanisms and Control Measures of Mature BF Resistance to Antimicrobial Agents in the Clinical Context. *ACS Omega* **2020**, *5* (36), 22684−22690.

(3) Brown, H. L.; Reuter, M.; Hanman, K.; Betts, R. P.; van Vliet, A. H. M. Prevention of BF Formation and Removal of Existing BFs by Extracellular DNases of Campylobacter jejuni. *PLoS One* **2015**, *10* (3), No. e0121680.

(4) Blackman, L. D.; Qu, Y.; Cass, P.; Locock, K. E. S. Approaches for the inhibition and elimination of microbial BFs using macromolecular agents. *Chem. Soc. Rev.* **2021**, *50* (3), 1587−1616.

(5) Highmore, C. J.; Melaugh, G.; Morris, R. J.; Parker, J.; Direito, S. O. L.; Romero, M.; Soukarieh, F.; Robertson, S. N.; Bamford, N. C. Translational challenges and opportunities in BF science: a BRIEF for the future. *npj BFs Microbiomes* **2022**, *8* (1), 68.

(6) Wang, Z.; de la Fuente-Núñez, C.; Shen, Y.; Haapasalo, M.; Hancock, R. E. W. Treatment of Oral Multispecies BFs by an Anti-BF Peptide. *PLoS One* **2015**, *10* (7), No. e0132512.

(7) Juárez-Cepeda, J.; Valenzuela, O.; Garibay-Valdez, E.; Velazquez, C.; Garibay-Escobar, A. Gene expression during the development of Mycobacterium smegmatis BFs on hydroxyapatite surfaces. *Int. Microbiol.* **2023**.

(8) O'Toole, G. A.; Kolter, R. Initiation of BF formation in Pseudomonas fluorescens WCS365 proceeds via multiple, convergent signalling pathways: a genetic analysis. *Mol. Microbiol.* **1998**, *28* (3), 449−461.

(9) Vogel, J.; Wakker-Havinga, M.; Setroikromo, R.; Quax, W. J. Immobilized Acylase PvdQ Reduces Pseudomonas aeruginosa BF Formation on PDMS Silicone. *Front. Chem.* **2020**, *8*, 54.

(10) Perez, C.; Lors, C.; Erable, B. Methodological approaches for the structural, chemical, and microbial analysis of microbial BFs developed on the surface of cementitious materials: Overview and future prospects. *Int. Biodeterior. Biodegrad.* **2022**, *175*, 105485.

(11) Anselme, K.; Davidson, P.; Popa, A. M.; Giazzon, M.; Liley, M.; Ploux, L. The interaction of cells and bacteria with surfaces structured at the nanometre scale. *Acta Biomater.* **2010**, *6* (10), 3824−3846.

(12) Karačić, S.; Modin, O.; Hagelia, P.; Persson, F.; Wilén, B. M. The effect of time and surface type on the composition of BF communities on concrete exposed to seawater. *Int. Biodeterior. Biodegrad.* **2022**, *173*, 105458.

(13) Tripathy, A.; Sen, P.; Su, B.; Briscoe, W. H. Natural and bioinspired nanostructured bactericidal surfaces. *Adv. Colloid Interface Sci.* **2017**, *248*, 85−104.

(14) Oda, S.; Tanikawa, A. A new plate-hanging method for BF quantification and its application to evaluate the role of surface hydrophobicity. *J. Microbiol. Methods* **2022**, *203*, 106608.

(15) Marcus, I. M.; Herzberg, M.; Walker, S. L.; Freger, V. Pseudomonas aeruginosa Attachment on QCM-D Sensors: The Role of Cell and Surface Hydrophobicities. *Langmuir* **2012**, *28* (15), 6396−6402.

(16) Merritt, J. H.; Kadouri, D. E.; O'Toole, G. A. Growing and analyzing static BFs. *Curr. Protoc. Microbiol.* **2011**, *22*, 1B.1.

(17) Filloux, A.; Ramos, J.-L. Pseudomonas methods and protocols. *Methods in Molecular Biology*; Springer, 2014; Vol. *1149*, p 293.

(18) Stiefel, P.; Rosenberg, U.; Schneider, J.; Mauerhofer, S.; Maniura-Weber, K.; Ren, Q. Is BF removal properly assessed? Comparison of different quantification methods in a 96-well plate system. *Appl. Microbiol. Biotechnol.* **2016**, *100* (9), 4135−4145.

(19) https://www.nanoscience.com/techniques/quartz-crystal-microbalance/ (accessed).

(20) Bard, A. J., Inzelt, G., Scholz, F., Eds. J BT—Electrochemical Dictionary; Springer: Berlin Heidelberg, 2008, pp 377−378.
(21) Lu, C.; Czanderna, A. W. *Applications of Piezoelectric Quartz Crystal Microbalances*; Elsevier Science, 2012.
(22) Sauerbrey, G. Verwendung von Schwingquarzen zur Wägung dünner Schichten und zur Mikrowägung. *Z. Phys.* **1959**, *155* (2), 206−222.
(23) Reviakine, I.; Johannsmann, D.; Richter, R. P. Hearing What You Cannot See and Visualizing What You Hear: Interpreting Quartz Crystal Microbalance Data from Solvated Interfaces. *Anal. Chem.* **2011**, *83* (23), 8838−8848.
(24) Wilson, C.; Lukowicz, R.; Merchant, S.; et al. Quantitative and Qualitative Assessment Methods for BF Growth: A Mini-review. *Res. Rev.: J. Eng. Technol.* **2017**, *6*(4).
(25) Afzal, A.; Mujahid, A.; Schirhagl, R.; Bajwa, S. Z.; Latif, U.; Feroz, S. Gravimetric Viral Diagnostics: QCM Based Biosensors for Early Detection of Viruses. *Chemosensors* **2017**, *5* (1), 7.
(26) Mujahid, A.; Mustafa, G.; Dickert, F. L. Label-Free Bioanalyte Detection from Nanometer to Micrometer Dimensions—Molecular Imprinting and QCMs †. *Biosensors* **2018**, *8* (2), 52.
(27) Alanazi, N.; Almutairi, M.; Alodhayb, A. N. A Review of Quartz Crystal Microbalance for Chemical and Biological Sensing Applications. *Sens. Imaging* **2023**, *24* (1), 10.
(28) Kartal, F.; Çimen, D.; Bereli, N.; Denizli, A. Molecularly imprinted polymer based quartz crystal microbalance sensor for the clinical detection of insulin. *Mater. Sci. Eng., C* **2019**, *97*, 730−737.
(29) Chernyshev, V. S.; Skliar, M. Quantification of Desiccated Extracellular Vesicles by Quartz Crystal Microbalance. *Biosensors* **2022**, *12* (6), 371.
(30) Mujahid, A.; Afzal, A.; Dickert, F. L. An Overview of High Frequency Acoustic Sensors-QCMs, SAWs and FBARs-Chemical and Biochemical Applications. *Sensors* **2019**, *19* (20), 4395.
(31) García-Bonillo, C.; Texidó, R.; Reyes-Carmenaty, G.; Gilabert-Porres, J.; Borrós, S. Study of the Human Albumin Role in the Formation of a Bacterial BF on Urinary Devices Using QCM-D. *ACS Appl. Bio Mater.* **2020**, *3* (5), 3354−3364.
(32) Ripa, R.; Shen, A. Q.; Funari, R. Detecting Escherichia coli BF Development Stages on Gold and Titanium by Quartz Crystal Microbalance. *ACS Omega* **2020**, *5* (5), 2295−2302.
(33) Olsson, A. L. J.; Mitzel, M. R.; Tufenkji, N. QCM-D for non-destructive real-time assessment of Pseudomonas aeruginosa BF attachment to the substratum during BF growth. *Colloids Surf., B* **2015**, *136*, 928−934.
(34) Ferreres, G.; Bassegoda, A.; Hoyo, J.; Torrent-Burgués, J.; Tzanov, T. Metal-Enzyme Nanoaggregates Eradicate Both Gram-Positive and Gram-Negative Bacteria and Their BFs. *ACS Appl. Mater. Interfaces* **2018**, *10* (47), 40434−40442.
(35) Asadishad, B.; Olsson, A. L. J.; Dusane, D. H.; Ghoshal, S.; Tufenkji, N. Transport, motility, BF forming potential and survival of Bacillus subtilis exposed to cold temperature and freeze-thaw. *Water Res.* **2014**, *58*, 239−247.
(36) Maurer-Jones, M. A.; Gunsolus, I. L.; Meyer, B. M.; Christenson, C. J.; Haynes, C. L. Impact of TiO2 nanoparticles on growth, BF formation, and flavin secretion in Shewanella oneidensis. *Anal. Chem.* **2013**, *85* (12), 5810−5818.
(37) Kaga, H.; Nakamura, A.; Orita, M.; Endo, K.; Akamatsu, M.; Sakai, K.; Sakai, H. Removal of a Model BF by Sophorolipid Solutions: A QCM-D Study. *J. Oleo Sci.* **2022**, *71* (5), 663−670.
(38) Ni, R.; Zhang, X.-B.; Liu, W.; Shen, G.-L.; Yu, R.-Q. Piezoelectric quartz crystal sensor array with optimized oscillator circuit for analysis of organic vapors mixtures. *Sens. Actuators, B* **2003**, *88* (2), 198−204.
(39) Escuderos, M. E.; Sánchez, S.; Jiménez, A. Quartz Crystal Microbalance (QCM) sensor arrays selection for olive oil sensory evaluation. *Food Chem.* **2011**, *124* (3), 857−862.
(40) Agustín, M. d. R.; Stengel, P.; Kellermeier, M.; Tücking, K. S.; Müller, M. Monitoring Growth and Removal of Pseudomonas BFs on Cellulose-Based Fabrics. *Microorganisms* **2023**, *11* (4), 892.
(41) Nadeau, L. J.; Barlow, D. E.; Hung, C.-S.; Biffinger, J. C.; Crouch, A. L.; Hollomon, J. M.; Ecker, C. D.; Russell, J. N.; Crookes-Goodson, W. J. Colonization and degradation of polyurethane coatings by Pseudomonas protegens BFs is promoted by PueA and PueB hydrolases. *Int. Biodeterior. Biodegrad.* **2021**, *156*, 105121.
(42) Nnabuife, O. O.; Ogbonna, J. C.; Anyanwu, C.; Ike, A. C. Population dynamics and crude oil degrading ability of bacterial consortia of isolates from oil-contaminated sites in Nigeria. *Int. Microbiol.* **2022**, *25* (2), 339−351.
(43) Wagner, M.; Ivleva, N. P.; Haisch, C.; Niessner, R.; Horn, H. Combined use of confocal laser scanning microscopy (CLSM) and Raman microscopy (RM): investigations on EPS-Matrix. *Water Res.* **2009**, *43* (1), 63−76.
(44) Liu, X.-Y.; Guo, S.; Bocklitz, T.; Rösch, P.; Popp, J.; Yu, H.-Q. Nondestructive 3D imaging and quantification of hydrated BF matrix by confocal Raman microscopy coupled with non-negative matrix factorization. *Water Res.* **2022**, *210*, 117973.
(45) Gayani, B.; Dilhari, A.; Kottegoda, N.; Ratnaweera, D. R.; Weerasekera, M. M. Reduced Crystalline BF Formation on Super-hydrophobic Silicone Urinary Catheter Materials. *ACS Omega* **2021**, *6* (17), 11488−11496.
(46) Al-Ahmad, A.; Wiedmann-Al-Ahmad, M.; Faust, J.; Bächle, M.; Follo, M.; Wolkewitz, M.; Hannig, C.; Hellwig, E.; Carvalho, C.; Kohal, R. BF formation and composition on different implant materials in vivo. *J. Biomed. Mater. Res., Part B* **2010**, *95B* (1), 101−109.
(47) Cabrera, J. N.; Rojas, G.; D'Accorso, N. B.; Lizarraga, L.; Negri, R. M. Membranes based on polyacrylamide coatings on metallic meshes prepared by a two-steps redox polymerization. Performance for oil-water separation and biofouling effects. *Sep. Purif. Technol.* **2020**, *247*, 116966.
(48) Chen, J.; Xu, K. Applications of atomic force microscopy in materials, semiconductors, polymers, and medicine: A minireview. *Instrum. Sci. Technol.* **2020**, *48* (6), 667−681.
(49) Cheah, Y. T.; Chan, D. J. C. A methodological review on the characterization of microalgal BF and its extracellular polymeric substances. *J. Appl. Microbiol.* **2022**, *132* (5), 3490−3514.
(50) Felz, S.; Vermeulen, P.; van Loosdrecht, M. C. M.; Lin, Y. M. Chemical characterization methods for the analysis of structural extracellular polymeric substances (EPS). *Water Res.* **2019**, *157*, 201−208.
(51) Shen, Y.; Huang, P. C.; Huang, C.; Sun, P.; Monroy, G. L.; Wu, W.; Lin, J.; Espinosa-Marzal, R. M.; Boppart, S. A.; Liu, W. T.; et al. Effect of divalent ions and a polyphosphate on composition, structure, and stiffness of simulated drinking water BFs. *npj BFs Microbiomes* **2018**, *4* (1), 15.
(52) Balouiri, M.; Sadiki, M.; Ibnsouda, S. K. Methods for in vitro evaluating antimicrobial activity: A review. *J. Pharm. Anal.* **2016**, *6* (2), 71−79.
(53) Howell, C. R.; Stipanovic, R. D. Suppression of Pythium ultimum-induced damping-off of cotton seedlings by Pseudomonas fluorescens and its antibiotic, pyoluteorin. *Phytopathology* **1980**, *70* (8), 712−715.
(54) https://www.biolinscientific.com/blog/why-are-overtones-important-in-qcm (accessed Jun28, 2022).
(55) Buttry, D. A.; Ward, M. D. Measurement of interfacial processes at electrode surfaces with the electrochemical quartz crystal microbalance. *Chem. Rev.* **1992**, *92* (6), 1355−1379.
(56) Dourado, A. H. B.; Silva, R. A.; Torresi, R. M.; Sumodjo, P. T. A.; Arenz, M.; Cordoba de Torresi, S. I. Kinetics, Assembling, and Conformation Control of L-Cysteine Adsorption on Pt Investigated by in situ FTIR Spectroscopy and QCM-D. *ChemPhysChem* **2018**, *19* (18), 2340−2348.
(57) Vogt, B. D.; Lin, E. K.; Wu, W.; White, C. C. Effect of Film Thickness on the Validity of the Sauerbrey Equation for Hydrated Polyelectrolyte Films. *J. Phys. Chem. B* **2004**, *108* (34), 12685−12690.
(58) Kananizadeh, N.; Rice, C.; Lee, J.; Rodenhausen, K. B.; Sekora, D.; Schubert, M.; Schubert, E.; Bartelt-Hunt, S.; Li, Y. Combined quartz crystal microbalance with dissipation (QCM-D) and

https://doi.org/10.1021/acsomega.3c08475
ACS Omega 2024, 9, 10445−10458

generalized ellipsometry (GE) to characterize the deposition of titanium dioxide nanoparticles on model rough surfaces. *J. Hazard. Mater.* **2017**, *322*, 118−128.
(59) Gieroba, B.; Krysa, M.; Wojtowicz, K.; Wiater, A.; Pleszczyńska, M.; Tomczyk, M.; Sroka-Bartnicka, A. The FT-IR and Raman Spectroscopies as Tools for BF Characterization Created by Cariogenic Streptococci. *Int. J. Mol. Sci.* **2020**, *21* (11), 3811.
(60) Sahu, R. K.; Salman, A.; Mordechai, S. Tracing overlapping biological signals in mid-infrared using colonic tissues as a model system. *World J. Gastroenterol.* **2017**, *23* (2), 286−296.
(61) Schmitt, J.; Flemming, H.-C. FTIR-spectroscopy in microbial and material analysis. *Int. Biodeterior. Biodegrad.* **1998**, *41* (1), 1−11.
(62) García, N.; Lamanna, M.; D'Accorso, N.; Dufresne, A.; Aranguren, M.; Goyanes, S. Biodegradable materials from grafting of modified PLA onto starch nanocrystals. *Polym. Degrad. Stab.* **2012**, *97* (10), 2021−2026.
(63) Whitfield, G. B.; Marmont, L. S.; Howell, P. L. Enzymatic modifications of exopolysaccharides enhance bacterial persistence. *Front. Microbiol.* **2015**, *6*, 471.
(64) Arciola, C. R.; Campoccia, D.; Ravaioli, S.; Montanaro, L. Polysaccharide intercellular adhesin in BF: structural and regulatory aspects. *Front. Cell. Infect. Microbiol.* **2015**, *5*, 7.
(65) Le Mauff, F.; Razvi, E.; Reichhardt, C.; Sivarajah, P.; Parsek, M. R.; Howell, P. L.; Sheppard, D. C. The Pel polysaccharide is predominantly composed of a dimeric repeat of α-1,4 linked galactosamine and N-acetylgalactosamine. *Commun. Biol.* **2022**, *5* (1), 502.
(66) Jennings, L. K.; Dreifus, J. E.; Reichhardt, C.; Storek, K. M.; Secor, P. R.; Wozniak, D. J.; Hisert, K. B.; Parsek, M. R. Pseudomonas aeruginosa aggregates in cystic fibrosis sputum produce exopolysaccharides that likely impede current therapies. *Cell Rep.* **2021**, *34* (8), 108782.
(67) Ramakrishnan, R.; Singh, A. K.; Singh, S.; Chakravortty, D.; Das, D. Enzymatic dispersion of BFs: An emerging biocatalytic avenue to combat BF-mediated microbial infections. *J. Biol. Chem.* **2022**, *298* (9), 102352.

https://doi.org/10.1021/acsomega.3c08475
ACS Omega 2024, 9, 10445−10458